RESEARCH ARTICLE

Design of hollow core step-index antiresonant fiber with stepped refractive indices cladding

Botao DENG[1], Chaotan SIMA (✉)[1], Hongyu TAN[1], Xiaohang ZHANG[1], Zhenggang LIAN[2], Guoqun CHEN[2], Qianqing YU[2], Jianghe XU[2], Deming LIU[1]

1 Next Generation Internet Access National Engineering Laboratory, School of Optical and Electronic Information, Huazhong University of Science and Technology, Wuhan 430074, China
2 Yangtze Optical Electronics Co., Ltd. (YOEC), Wuhan 430205, China

Abstract With the benefits of low latency, wide transmission bandwidth, and large mode field area, hollow-core antiresonant fiber (HC-ARF) has been a research hotspot in the past decade. In this paper, a hollow core step-index antiresonant fiber (HC-SARF), with stepped refractive indices cladding, is proposed and numerically demonstrated with the benefits of loss reduction and bending improvement. Glass-based capillaries with both high ($n = 1.45$) and low (as low as $n = 1.36$) refractive indices layers are introduced and formatted in the cladding air holes. Using the finite element method to perform numerical analysis of the designed fiber, results show that at the laser wavelengths of 980 and 1064 nm, the confinement loss is favorably reduced by about 6 dB/km compared with the conventional uniform cladding HC-ARF. The bending loss, around 15 cm bending radius of this fiber, is also reduced by 2 dB/km. The cladding air hole radius in this fiber is further investigated to optimize the confinement loss and the mode field diameter with single-mode transmission behavior. This proposed HC-SARF has great potential in optical fiber transmission and high energy delivery.

Keywords antiresonant fiber (ARF), stepped refractive indices, confinement loss, bending loss, laser pumping

1 Introduction

Since the transmission of light in solid-core fibers is limited by the loss and nonlinearity of the core material [1], hollow-core fibers have received extensive attention.

According to different wave-guiding principles, hollow core microstructure fibers can basically be divided into several categories: hollow core Bragg fiber, hollow core photonic band gap fiber, and hollow core antiresonant fiber (HC-ARF) [2–5]. The HC-ARF has relatively simple geometry. It also currently has two acknowledged light guiding mechanisms found in research: the principle of antiresonant reflection [6] and the mode coupling theory between the cladding and core [7], for example. HC-ARF has some transmission properties that are not inferior to those of the photonic bandgap fiber. Also, its geometry indicates great simplification of the fabrication process. In addition, it has great prospects in practical applications. Researchers are mainly working on the low confinement loss HC-ARF, with birefringence for sensing, or large mode field area for high-power delivery [8–19].

The primary HC-ARF is known as the holey photonic crystal fiber with Kagome cladding reported by Benabid et al. [8]. Because of its advantages, such as wide bandwidth [9], it has gained strong worldwide interest and has gradually developed into two types: the hypocycloid and negative curvature. The hypocycloid Kagome HC-ARF has been continuously modified and improved to reduce transmission loss and to obtain a loss below 10 dB/km [10,11]. As for the negative curvature HC-ARF, it is mainly developed to achieve mid-to-far infrared light propagation and to reach a loss of tens dB/km levels [12,13]. Meanwhile, these structures came across some challenges to further reduce the overall loss due to Fano resonance [14]. To overcome the loss limitation, a nodeless HC-ARF has been proposed and demonstrated. The transmission loss of the nodeless HC-ARF, in some wavelength bands, could reach several decibels per km [15]. It is also proved that the nodeless HC-ARF, with 6–8 cladding tubes, performs superior for low-loss transmission [7].

Recently, based on the nodeless HC-ARF, the multilayer and multiring antiresonance structure has been proposed to further reduce the transmission confinement loss. Hasan et al. reported a negative curvature HC-ARF with nested elliptical elements in the cladding tubes, showing a confinement loss below 0.1 dB/km between 1000 and 1500 nm [16]. Gao et al. reported a conjoined-tube HC-ARF with about 2 dB/km confinement loss at 1512 nm [17]. Sakr et al. presented a nested nodeless HC-ARF with 700 nm wavelength bandwidth, and 6.6 dB/km confinement loss at 1550 nm [18]. To be noted, the above-mentioned HC-ARF literature focused on the geometry modification and innovation, with merely single uniform silica glass material ($n \approx 1.45$).

In this paper, a hollow core step-index antiresonant fiber (HC-SARF) is proposed and numerically demonstrated. Varied from the conventional uniform index HC-ARF, high ($n_1 = 1.45$) and low (as low as $n_2 = 1.36$) refractive indices layers are combined into the tube wall of the cladding air hole. Using the finite element method (FEM) to perform numerical analysis of the designed fiber, the confinement loss is favorably reduced by about 6 dB/km at the pumping laser and ultrafast laser wavelengths (980 and 1064 nm), when compared with conventional structures. The bending loss, around 15 cm bending radius, is also reduced by 2 dB/km. The cladding air hole radius in this HC-SARF is further investigated to optimize the confinement loss and the mode field diameter with single-mode transmission characteristics of the designed fiber. By changing the lower refractive index n_2 of the air tube wall and the cladding air hole radius r, the light propagation performance is further investigated and optimized. This work theoretically investigates the influence of the refractive index, the thickness of the second material, as well as the cladding tube size on fiber properties and the comparison with the conventional single-layer fiber for the loss and bending improvement. This designed holey fiber has great potential in low-loss transmission and high-power delivery for ultrafast lasers and pumping lasers.

2   Principles and methods

Litchinitser et al. proposed an antiresonant reflecting optical waveguide (ARROW) model for low-index core optical waveguides [6]. Based on the low-loss seven tubes nodeless HC-ARF [19], the nodeless tubular fiber (comprising a single ring of seven tubes) is primarily employed in the design. Innovatively, we introduced the stepped layers with high and low refractive indices in the cladding tube wall of the conventional structure.

As for the light guiding principle of the conventional single-layer cladding tube, Litchinitser et al. have given a theoretical explanation as follows [6]:

$$2nt\sqrt{n^2-1} = \frac{m}{2}\lambda_m, \ m = 1,2,3,... \tag{1}$$

$$\lambda_m = \frac{m}{4}nt\sqrt{n^2-1}, \ m = 1,2,3,... \tag{2}$$

where n and t are the refractive index and thickness of the cladding tube, respectively. If m is odd number, the light with corresponding λ_m will be reflected at the cladding interface into the core. This will result in a high transmission coefficient in the core, as the guided light. If m is even number, the light with corresponding λ_m will leak into the cladding with a low transmission coefficient in the core.

For the step indices layer tube, Belardi et al. also proposed a theoretical analysis method by equivalently considering a two-layer step refractive index tube, as a single-layer tube with refractive index n_{eq}, and thickness t_{eq} as follows [20]:

$$n_{eq} = n_1\frac{S_1}{S_1+S_2} + n_2\frac{S_2}{S_1+S_2}, \tag{3}$$

$$t_{eq} = t_1 + t_2, \tag{4}$$

where n_1 and n_2 are the refractive index of the two layers, t_1 and t_2 are the thickness of the two layers, and S_1 and S_2 are the surfaces occupied by the two layers.

Figure 1 shows the principle of longitudinal structure schematic of the designed HC-SARF, based on the ARROW model. The high (n_1) and low (n_2) refractive index layers of the cladding, illustrated as gray areas in Fig. 1, can be considered an Fabry–Pérot (FP) resonator. If the light with wavelength λ_1 in Fig. 1 could satisfy the resonant condition, the light will leak into the cladding with a low transmission coefficient in the core. If the light with wavelength λ_2 varies from the resonant condition, the light will be reflected at the cladding interface into the core. This will result in a high transmission coefficient in the core as the guided light.
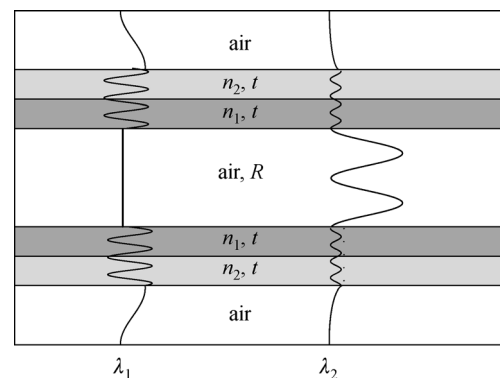
Fig. 1   Longitudinal structure schematic of the stepped refractive index HC-ARF based on the ARROW model
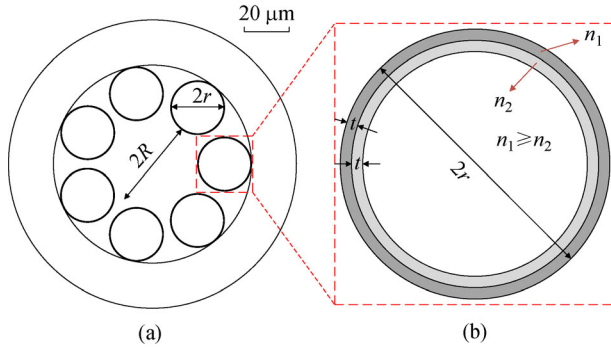
Fig. 2   Cross section of HC-SARF with stepped high and low refractive indices cladding. (a) Overall transverse geometry. (b) Enlarged stepped indices area
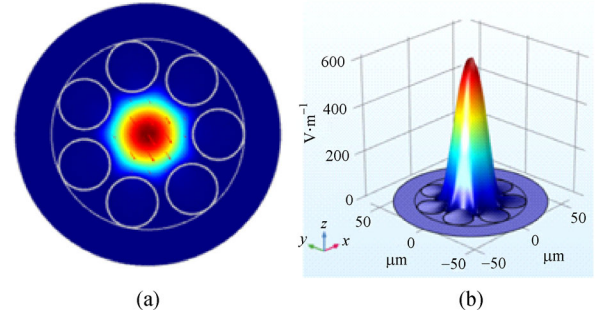

Fig. 3   Fundamental mode field distribution of the designed HC-SARF with stepped refractive indices cladding. (a) Two-dimensional image. (b) Three-dimensional profile

Figure 2 shows the cross-sectional geometry of the proposed HC-SARF. The core is filled with air with a central air hole radius of R = 20.1 μm. The cladding consists of seven identical non-contact air tubes with an outer radius of r = 12 μm. The air tube wall is composed of silica and similar glass material, and it is divided into two layers, both with a thickness of t = 0.18 μm. The outer layer has a higher refractive index layer with n_1 = 1.45, while the inner layer has a lower refractive index of n_2 = 1.36–1.44. The available refractive index value of glass materials can be found in some related research and literatures [21]. With these parameters, the FEM is utilized to perform numerical analysis of the designed fiber. The confinement loss, the bending loss, as well as the single-mode transmission characteristics, are analyzed and discussed.

3   Simulation and discussion

The fundamental mode of the designed HC-SARF is initially simulated. First, the low refractive index region, n_2 of the cladding air hole tube wall, is changed from 1.45, 1.43, and 1.41 to 1.36, while the n_1 is set to 1.45. It becomes a conventional HC-ARF when n_2 = 1.45. Secondly, the cladding air hole radius r is analyzed to further discuss and optimize the fiber characteristics. Figure 3 shows the circular-symmetric Gaussian shape fundamental mode field distribution of the designed HC-ARF, which indicates a promising light confinement and guidance in the air core.

3.1   Confinement loss with refractive index contrast

To obtain improved transmission characteristics beyond the conventional HC-ARF, we simulated and analyzed the confinement loss and the bending loss of the HC-SARF. This process was carried out by varying the refractive index n_2 of the inner layer of the cladding air tube wall. Figure 4
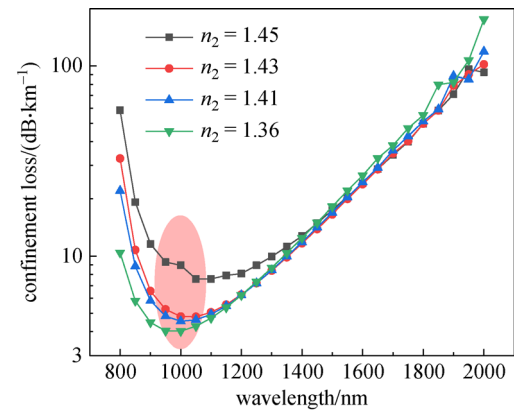
Fig. 4   Confinement loss with respect to wavelength for the designed HC-SARF with different indices contrast

shows the fundamental mode confinement loss of the designed HC-SARF from 800 to 2000 nm, while changing inner layer refractive index n_2. It is apparent that the confinement loss decreases with lower n_2 between 800 and 1100 nm. Especially for the pumping lasers and the ultrafast laser wavelengths of 980 and 1064 nm, the confinement loss is significantly reduced. Therefore, it is concluded that the designed HC-ARF, with stepped refractive indices cladding, can achieve minor confinement loss.

### 3.2   Bending loss with refractive index contrast

Due to coupling between cladding modes and core modes, the conventional HC-ARF usually comes across with serious bending issues [22]. It is acknowledged that there is trade-off between bending loss and confinement loss of the HC-ARF. To reduce the confinement loss, the core diameter of the HC-ARF is generally ten times the wavelength value. This leads to the sharply increased bending loss, once the bending radius is below 10 cm. This effect will seriously restrict the practical applications of the HC-ARF. The bending loss (BL) in holey fiber could be derived as [23]

$$n_{eq}(x,y) = n(x,y)e^{\frac{x}{R_b}}, \qquad (5)$$

$$BL = \frac{20}{\ln 10} \cdot \frac{2\pi}{\lambda} Im(n_{eff}) = 8.686 \times \frac{2\pi}{\lambda} Im(n_{eff}), \qquad (6)$$

where $n_{eq}(x,y)$ is the equivalent cross-sectional refractive index distribution of the bending HC-SARF, $n(x,y)$ is the equivalent cross-sectional refractive index of straight HC-SARF, x is coordinate of the bending direction, R_b is bending radius, and n_{eff} is the effective refractive index of the fundamental mode.

Based on Eqs. (5) and (6), the bending loss of the proposed HC-SARF is simulated and analyzed with respect to the bending radius. Figure 5 shows the shifted fundamental mode field distribution of the bending HC-SARF, and the bending orientation is along the positive direction of x-axis. Figure 6 presents the bending loss of the designed HC-SARF with different n_2 at the operating wavelength of 1064 nm, where it exhibits the minimum confinement loss in Fig. 4. As shown in Fig. 6(a), the designed HC-SARF has lower bending loss with the decreased n_2. When $n_2 = 1.36$, the bending loss is reduced by about 2 dB for the bending radius between 14 and 20 cm, as shown in Fig. 6(b). Therefore, it could be
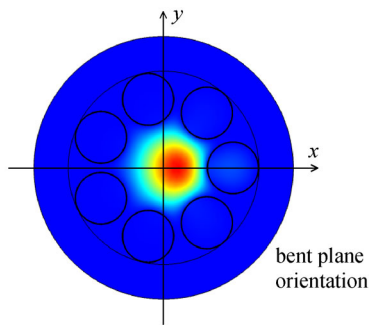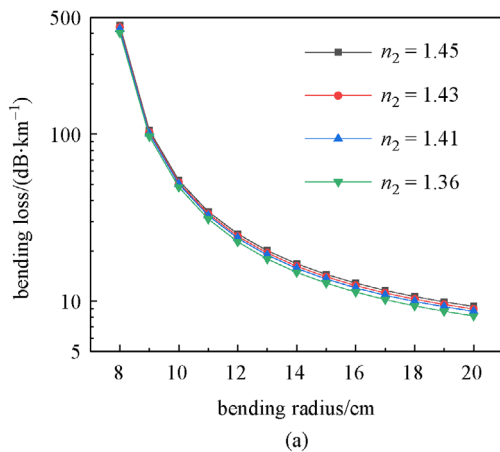
concluded that the designed high and low stepped refractive indices cladding has a strong contribution toward reducing the bending loss of the HC-ARF.

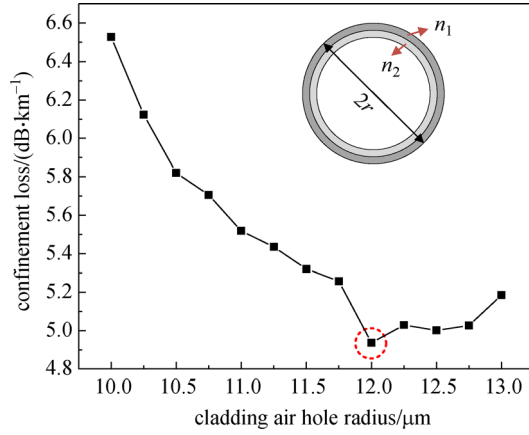### 3.3 Confinement loss with cladding air hole radius

The confinement loss of this HC-SARF could also be modified and optimized with the cladding air hole radius, if in the setting of the lower refractive index, $n_2 = 1.43$, and in the central air core radius, $R = 20.1$ μm. Figure 7 illustrates the relationship between the fundamental mode confinement loss and the cladding air hole radius. The confinement loss first decreases and then rises with the increased r and reaches the minimum value at $r = 12$ μm. Hence, it is recommended to have the air hole radius equivalent to around 12 μm in this design.

3.4 Single-mode transmission performance related to cladding air hole radius

While maintaining the lower refractive index $n_2 = 1.43$ and the central air core radius $R = 20.1$ μm, by changing the radius r of the cladding air hole, the mode coupling theory is employed [7] to investigate the influence of the cladding air hole radius on the single mode maintaining and fundamental mode field diameter of the designed HC-SARF. Figure 8(a) depicts the effective refractive index n_{eff} of LP_{01} and LP_{11} mode in the core, as well as the LP_{01} mode in the cladding from 800 to 2000 nm, and the cladding air hole radius $r = 11$, 12, and 13 cm. Considering the data in Fig. 8(a), the n_{eff} of $LP_{11\text{-}core}$ (in red color) and $LP_{01\text{-}cladding}$ (in blue color) is adjacent, which indicates that the higher-order mode $LP_{11\text{-}core}$ in the core is more likely to be coupled into the cladding mode $LP_{01\text{-}cladding}$. Therefore, the fundamental core mode $LP_{01\text{-}core}$ could be well maintained. Figure 8(b) shows the detailed n_{eff} difference between $LP_{11\text{-}core}$ and $LP_{01\text{-}cladding}$, with respect to the cladding air hole radius. As the cladding air hole radius r increases from 10 to 13 cm, the n_{eff} contrast decreases,

**Fig. 5** Fundamental mode field distribution of the bending HC-SARF in the x-axis orientation
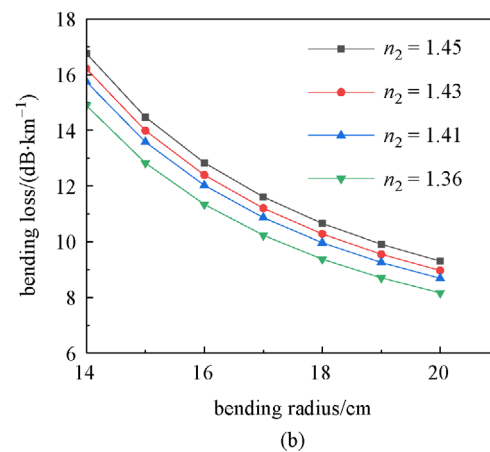
Fig. 6 Bending loss with respect to bending radius for the designed HC-SARF. (a) Between 8 and 20 cm. (b) Enlarged section between 14 and 20 cm

Fig. 7 Fundamental mode confinement loss with respect to cladding air hole radius r for the designed HC-SARF
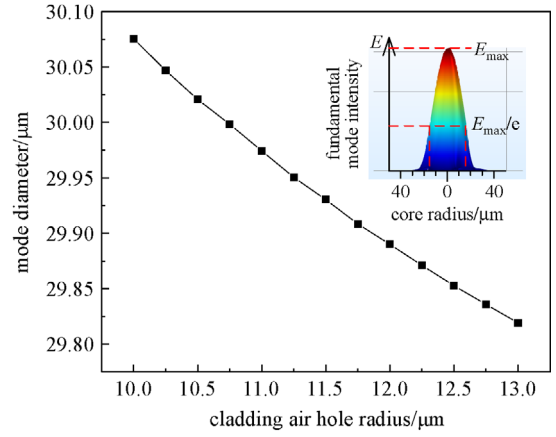
Fig. 9 Fundamental mode field diameter with respect to cladding air hole radius for the designed HC-SARF
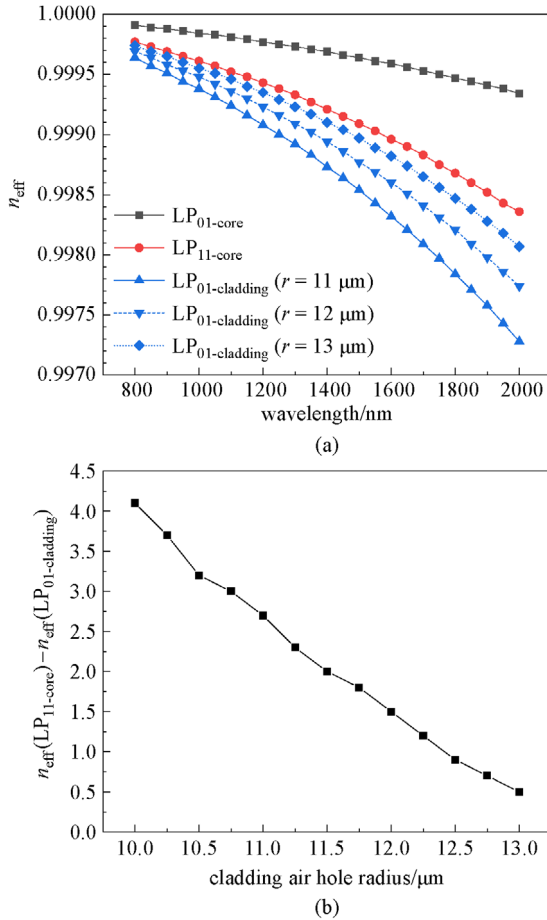
Fig. 8 Mode effective refractive index n_{eff} of the core and cladding mode. (a) Relationship with wavelengths for $r = 11$, 12, and 13 cm. (b) Detailed n_{eff} contrast between $LP_{11-core}$ and $LP_{01-cladding}$

allowing $LP_{11-core}$ to be easily coupled with the $LP_{01-cladding}$. This results in maintaining transmission of the single mode.

Considering the 1064-nm light in laser pumping applications, the high-power density delivery capability is essential for this HC-SARF implementation. Here, the mode field diameter (MFD) is also analyzed and discussed for the designed HC-SARF. Figure 9 shows the relationship between the $LP_{01-core}$ MFD and the cladding air hole radius. The MFD remains around a level of 30 μm, and it slightly decreases with the increased r.

Originated from the conventional stacking and drawing process for photonic crystal fibers (PCFs), current fabrication techniques for the HC-ARF can achieve the single-layer tube thickness of 200 to 300 nm and a low confinement loss [17–20]. Moreover, the fluoride-doped glass material has shown the decreased refractive index to be below 1.36 [21]. Hence, it is possible to develop fiber fabrication methods applied to the proposed design, by introducing material deposition techniques and stacking and drawing the PCF fabrication process.

4   Conclusions

A unique HC-SARF design, with stepped refractive indices cladding, has been proposed and numerically analyzed. This work theoretically investigates the influence of the refractive index and the thickness of the step-index material, as well as the cladding tube size on fiber properties and the comparison with the conventional single-layer HC-ARF. With a dedicated and optimized design of the fiber geometry, it shows the advanced light transmission characteristics, such as reduced confinement loss and bending loss. The confinement loss is reduced by about 6 dB/km compared with the conventional HC-ARF

at the 980 and 1064 nm wavelength for pumping lasers and ultrafast lasers. The bending loss (around 14 cm bending radius of this fiber) is also reduced by 2 dB/km. Since the design concept is universal for the antiresonant structure, it can be directly applied to ultra-low loss HC-ARF and for high-power delivery applications, showing great potential in the fields of optical communication and laser delivery.

References

1. Wang Y Y, Wheeler N V, Couny F, Roberts P J, Benabid F. Low loss broadband transmission in hypocycloid-core Kagome hollow-core photonic crystal fiber. Optics Letters, 2011, 36(5): 669–671

2. Wang Y, Yan G, Lian Z, Wu C, He S. Liquid-level sensing based on a hollow core Bragg fiber. Optics Express, 2018, 26(17): 21656–21663

3. Jin W, Ju J, Ho H L, Hoo Y L, Zhang A L. Photonic crystal fibers, devices, and applications. Frontiers of Optoelectronics, 2013, 6(1): 3–24

4. Chen W, Li J Y, Lu P X. Progress of photonic crystal fibers and their applications. Frontiers of Optoelectronics, 2009, 2(1): 50–57

5. Knight J C. What do you see in photonic crystal fibers? Frontiers of Optoelectronics in China, 2010, 3(1): 2–8

6. Litchinitser N M, Abeeluck A K, Headley C, Eggleton B J. Antiresonant reflecting photonic crystal optical waveguides. Optics Letters, 2002, 27(18): 1592–1594

7. Vincetti L, Setti V. Waveguiding mechanism in tube lattice fibers. Optics Express, 2010, 18(22): 23133–23146

8. Benabid F, Knight J C, Antonopoulos G, Russell P S J. Stimulated Raman scattering in hydrogen-filled hollow-core photonic crystal fiber. Science, 2002, 298(5592): 399–402

9. Couny F, Benabid F, Light P S. Large-pitch kagome-structured hollow-core photonic crystal fiber. Optics Letters, 2006, 31(24): 3574–3576

10. Debord B, Alharbi M, Benoît A, Ghosh D, Dontabactouny M, Vincetti L, Blondy J M, Gérôme F, Benabid F. Ultra low-loss hypocycloid-core Kagome hollow-core photonic crystal fiber for green spectral-range applications. Optics Letters, 2014, 39(21): 6245–6248

11. Wheeler N V, Bradley T D, Hayes J R, Gouveia M A, Liang S, Chen Y, Sandoghchi S R, Abokhamis Mousavi S M, Poletti F, Petrovich M N, Richardson D J. Low-loss Kagome hollow-core fibers operating from the near- to the mid-IR. Optics Letters, 2017, 42 (13): 2571–2574

12. Pryamikov A D, Biriukov A S, Kosolapov A F, Plotnichenko V G, Semjonov S L, Dianov E M. Demonstration of a waveguide regime for a silica hollow–core microstructured optical fiber with a negative curvature of the core boundary in the spectral region $> 3.5~\mu$m. Optics Express, 2011, 19(2): 1441–1448

13. Yu F, Knight J C. Spectral attenuation limits of silica hollow core negative curvature fiber. Optics Express, 2013, 21(18): 21466–21471

14. Vincetti L, Setti V. Extra loss due to Fano resonances in inhibited coupling fibers based on a lattice of tubes. Optics Express, 2012, 20 (13): 14350–14361

15. Debord B, Amsanpally A, Chafer M, Baz A, Maurel M, Blondy J M, Hugonnot E, Scol F, Vincetti L, Gérôme F, Benabid F. Ultralow transmission loss in inhibited-coupling guiding hollow fibers. Optica, 2017, 4(2): 209–217

16. Hasan M I, Akhmediev N, Chang W. Positive and negative curvatures nested in an antiresonant hollow-core fiber. Optics Letters, 2017, 42(4): 703–706

17. Gao S F, Wang Y Y, Ding W, Jiang D L, Gu S, Zhang X, Wang P. Hollow-core conjoined-tube negative-curvature fibre with ultralow loss. Nature Communications, 2018, 9(1): 2828

18. Sakr H, Hong Y, Bradley T D, Jasion G T, Hayes J R, Kim H, Davidson I A, Numkam Fokoua E, Chen Y, Bottrill K R H, Taengnoi N, Wheeler N V, Petropoulos P, Richardson D J, Poletti F. Interband short reach data transmission in ultrawide bandwidth hollow core fiber. Journal of Lightwave Technology, 2020, 38(1): 159–165

19. Hayes J R, Fokoua E N, Petrovich M N, Richardson D J, Poletti F, Sandoghchi S R, Bradley T D, Liu Z X, Slavik R, Gouveia M A, Wheeler N V, Jasion G, Chen Y. Antiresonant hollow core fiber with an octave spanning bandwidth for short haul data communications. Journal of Lightwave Technology, 2017, 35(3): 437–442

20. Belardi W, De Lucia F, Poletti F, Sazio P J. Composite material hollow antiresonant fibers. Optics Letters, 2017, 42(13): 2535–2538

21. Weber M J, Cline C F, Smith W L, Milam D, Heiman D, Helpworth R W. Measurements of the electronic and nuclear contributions to the nonlinear refractive index of beryllium fluoride glasses. Applied Physics Letters, 1978, 32(7): 403–405

22. Belardi W, Knight J C. Effect of core boundary curvature on the confinement losses of hollow antiresonant fibers. Optics Express, 2013, 21(19): 21912–21917

23. Setti V, Vincetti L, Argyros A. Flexible tube lattice fibers for terahertz applications. Optics Express, 2013, 21(3): 3388–3399

Botao Deng received the B.S. degree from Huazhong University of Science and Technology, China in 2020. Now he is working toward his M.S. degree in Huazhong University of Science and Technology and his research interests include optical communication and fiber sensing.

Chaotan Sima is an Associate Professor and Ph.D. supervisor in School of Optical and Electronic Information at Huazhong University of Science and Technology, and Next Generation Internet Access National Engineering Laboratory, China. In 2006, he graduated from Huazhong University of Science and Technology with the distinguished bachelor degree. In 2013, He obtained the Ph.D. degree in Optoelectronics from Optoelectronics

Research Centre in University of Southampton, UK, with the project of planar Bragg grating devices for advanced optical communication systems. After the industry experience as a R&D director, he joined School of Optical and Electronic Information in Huazhong University of Science and Technology in 2014. He has been awarded the Marie-Curie Fellowship in 2019. His research interests include integrated Bragg grating devices and implementation, special fiber design, and optical gas sensing. He has authored/co-authored over 50 international publications, some of which are invited. He has been the PI for over 10 grants including projects from the National Natural Science Foundation of China and National Key National Key Research and Development Project. He serves as an editorial member of *Optical and Quantum Electronics*, and a frequent reviewer of tens of OSA, IEEE and IET technical journals. He is also the TPC member of several international optoelectronic conferences, as well as a member of OSA, IEEE and CSOE.

Hongyu Tan is a master student in School of Optical and Electronic Information at Huazhong University of Science and Technology, and Next Generation Internet Access National Engineering Laboratory, China since 2019. He graduated from Huazhong University of Science and Technology with a bachelor degree in 2019. His research interests include design of highly-birefringent hollow core photonic bandgap fiber and integrated Bragg grating devices.

Zhenggang Lian, Ph.D., professor-level senior engineer, CTO of Yangtze Optical Electronic Co., Ltd., director of Wuhan Calibration and Testing Center of National Defense Science and Industry Optoelectronics Level One Metrology Station. He has been awarded Hubei Province "Hundred Talents Program" expert and Wuhan "3551 Optics Valley Talent" expert, as well as a part-time professor at Huazhong University of Science and Technology, China. He graduated from University of Nottingham, UK, with a doctorate degree in Electrical and Electronic Engineering. He worked as postdoctoral research fellow at Optoelectronics Research Centre in University of Southampton, UK. He has over 15 years of experience in the synthesis and processing of special optical fiber materials and the preparation and testing of special structure optical fibers. He has published more than 50 research articles and been cited over 200 times. He is a reviewer of many international optical journals. He is leading the team to be selected as "Hubei Federation of Returned Overseas Chinese-National Returned Overseas Chinese Innovation Team". He participated in general projects of the National Natural Science Foundation of China and held four invention patents.

Deming Liu is a Professor at Huazhong University of Science and Technology and director of Next Generation Internet Access National Engineering Laboratory, China since 2008. In 1984, he obtained a master degree and worked as a teacher at Huazhong Institute of Technology, China. From 1994 to 1996, he was the Visiting Professor at University of Duisburg, Germany. In 1999, he obtained the Ph.D. degree from Huazhong University of Science and Technology. He was the Visiting Professor at Nanyang Technological University, Singapore from 1999 to 2000. From 2000 to 2005, he was the director of the Optoelectronics Department of Huazhong University of Science and Technology. From 2005 to 2008, he was Deputy Dean of School of Optoelectronic Science and Engineering, Huazhong University of Science and Technology. His research interests include optical communication devices and systems, optical access and wireless access, and optical sensing and Internet of Things. He presided over and undertook more than 50 national, provincial and ministerial projects including 973, 863, science and technology support plan, national natural science fund key projects and international cooperation key projects, and won one second prize of the National Technical Invention Award, one third prize of state award for inventions, one gold medal at the Geneva International Invention Exhibition, one first prize for technological invention in Hubei Province, one first prize for natural science from the Ministry of Education, four other provincial and ministerial second prizes; more than 30 scientific and technological achievements passed provincial and ministerial appraisal, applied for more than 50 national invention patents (including more than 20 authorized), published nearly 200 academic papers, including more than 100 papers included in SCI, published three national planning textbooks and one monograph.